Available online at www.sciencedirect.com
SCIENCE DIRECT®
Solar Energy Materials & Solar Cells
ELSEVIER
Solar Energy Materials & Solar Cells 82 (2004) 315–330
www.elsevier.com/locate/solmat

Nano-structured CdTe, CdS and TiO_2 for thin film solar cell applications

R.S. Singh[a], V.K. Rangari[b], S. Sanagapalli[a], V. Jayaraman[a], S. Mahendra[a], V.P. Singh[a,*]

[a] *Center for Micro-Magnetic and Electronic Devices, Department of Electrical and Computer Engineering, University of Kentucky, 453 F. Paul Anderson Tower, Lexington, KY 40506-0046, USA*
[b] *Center for Advanced Materials, Tuskegee University, Tuskegee, AL, USA*

Abstract

Nano-crystalline CdTe and nano-structured CdS films in crystalline, porous and fiber forms were deposited on ITO-coated glass substrates. CdTe films exhibited a typical particle size of 10 nm and a blue shift in the absorption with an effective band gap of 2.8 eV. CdS films exhibited a typical particle size of 15 nm and an effective band gap of 2.98 eV. Also, porous CdS and porous TiO_2 films were deposited on plastic substrates by a self-assembly method. Typical pore sizes were 80 and 70 nm, respectively. These can be used in nano-structured solar cell configuration where the pores are filled with a suitable absorber material. Additionally, CdS fibers and nano-crystalline films of TiO_2 on plastic substrates were fabricated. Typical particle size in TiO_2 was 10 nm and CdS fibers were about 80 nm wide and 1.5 μm long.

Keywords: CdS/CdTe solar cell; Nano-crystalline; Nano-porous; Thin film; TiO_2

1. Introduction

Many nano-structured materials are now being investigated for their potential applications in photovoltaic, electro-optical, micromechanical and sensor devices [1–3]. Our interest lies in taking advantage of the benefits offered by nanotechnology to make inexpensive and efficient solar cells on a large scale. To this end, nano-structured layers in thin film solar cells offer three important advantages. First, due to multiple reflections, the effective optical path for absorption is much larger than the actual film thickness. Second, light generated electrons and holes need to travel

*Corresponding author. Tel.: +1-859-257-3092; fax: +1-859-257-3092.
E-mail address: vsingh@engr.uky.edu (V.P. Singh).

0927-0248/$ - see front matter © 2004 Elsevier B.V. All rights reserved.
doi:10.1016/j.solmat.2004.02.006

over a much shorter path and thus recombination losses are greatly reduced. As a result, the absorber layer thickness in nano-structured solar cells can be as thin as 150 nm instead of several micrometers in the traditional thin film solar cells [4]. Third, the energy band gap of various layers can be tailored to the desired design value by varying the size of nano-particles. This allows for more design flexibility in the absorber and window layers in the solar cell. In particular nano-structured CdS, CdTe and TiO_2 are of interest as window and absorber layers in thin film solar cells [5–10]. Fabrication and characterization of these films constitute the focus of this work.

Production of large-area solar cells would also require a process for inexpensive fabrication of large periodic arrays of semiconductor nanostructures that will allow for (a) controlled variations in the size and composition of the nanostructures, (b) encapsulation of the semiconductor nanostructures in a rugged host material, (c) flexibility to use a variety of substrate materials, and, preferably, (d) compatibility with standard silicon fabrication techniques. Self-assembly is such a process. We have used the self-assembly process to fabricate a variety of nano-structured films including CdTe and CdS on ITO-coated glass substrates. In addition nano-porous CdS and TiO_2 films were fabricated on a plastic substrate with a view to making devices on a lightweight, flexible substrate. Fabrication techniques and material characteristics of these films and their applications to solar cells are described below. Results on CdTe, CdS and TiO_2 are presented in Sections 2, 3 and 4, respectively.

2. Nano-crystalline CdTe films

Nano-crystalline CdTe films are of interest because of their potential applications as n-type window layers in a p–n homojunction thin film CdTe solar cell (Fig. 1) and in electroluminescent displays devices [11–13]. CdTe nanocrystals were prepared by microwave-assisted synthesis and films were cast from colloidal solutions containing

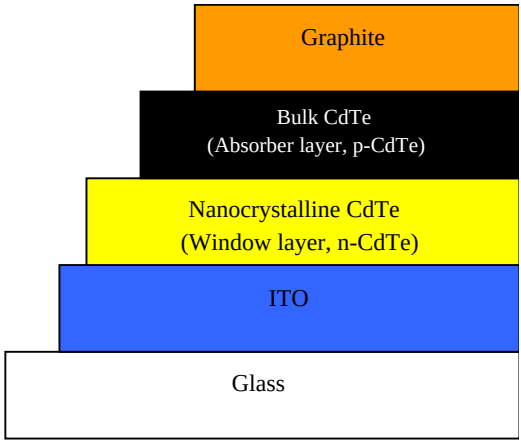

Fig. 1. Device configuration of a Glass/ITO/n-Nano-CdTe/p-bulk CdTe/graphite solar cell.

nano-CdTe. These films were characterized by optical absorption, photoluminescence spectroscopy, profilometer and scanning electron microscopy on glass and plastic substrates for various conditions. The microwave-assisted synthesis was carried out in a custom made 1000 W/2.45 GHz Sharp-R21-HT-microwave oven supplied by Microwave Specialties Inc., USA. The oven's cavity was modified to include a complete refluxing system. In the present experiment, a 250 ml long neck flask with a refluxing condenser assembly was used. All the reactions were carried out with continuous heating at 50% power of the 1000 W, under flow of argon gas. A coolant liquid ($\sim 5^{\circ}C$) was circulated through the refluxing condenser throughout the experiment. A few glass capillary tubes (3–5) were also added to the reaction mixture to avoid the sudden liquid bumps.

1 g of cadmium (II) acetate dihydrate was dissolved in 100 ml of ethylene glycol and then stoichiometric quantity (0.40 g) of tellurium powder was added. The system was purged for 10 min with argon and the reaction vessel was exposed to microwave radiation continuously for 30 min. At this stage, the reaction mixture turned to grayish color then the reaction mixture was diluted with ethanol to precipitate and centrifuged at 5000 rpm. The precipitate was further washed with ethanol several times and dried overnight under vacuum.

The nano-crystalline CdTe powder thus obtained by microwave assisted synthesis was dispersed in methanol and coated on to ITO-coated glass. The resulting films were examined with a FE-SEM and the electron micrograph shows a particle size of about 10 nm (Fig. 2). The UV–VIS spectra recorded on this film shows a blue shift in

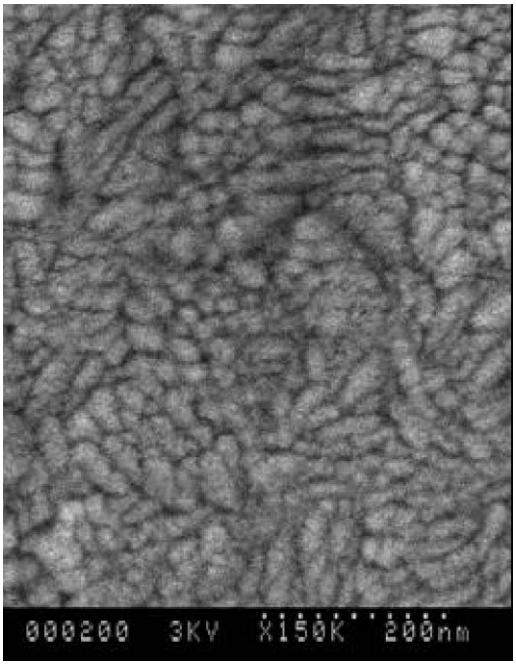

Fig. 2. FE-SEM image of a nanocrystalline CdTe film on ITO-coated glass substrate.

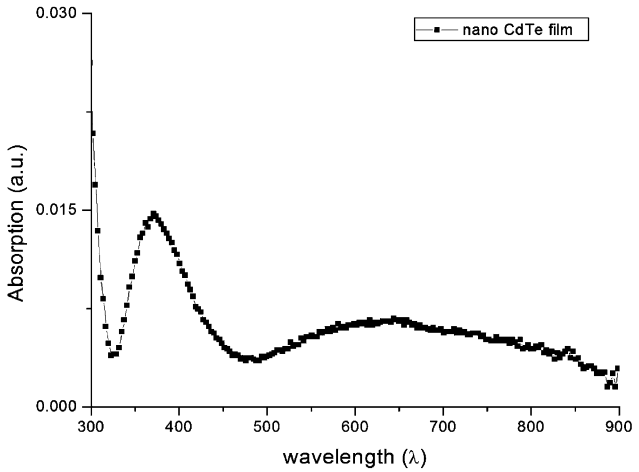

Fig. 3. Absorption spectrum of a nanocrystalline CdTe film on ITO-coated glass substrate.

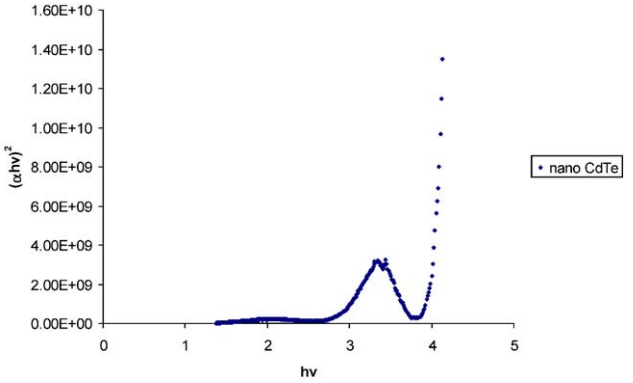

Fig. 4. Tauc's law calculation for a nanocrystalline CdTe film on ITO-coated glass substrate.

absorption due to smaller particle size (Fig. 3). Tauc's relation was used to determine the effective band gap (E_{eff}) for the films. $(\alpha hv)^2$ was plotted against hv (Fig. 4) and E_{eff} was obtained by extrapolation to zero value of $(\alpha hv)^2$. Band gap estimate using Tauc's law indicates a value of about 2.8 eV as compared to a bulk CdTe band gap of 1.5 eV. This increased band gap makes CdTe a good candidate for electroluminescent display devices [11–13] and for window layers in n-CdTe/P-CdTe homojunction solar cells (Fig. 1).

3. Nano-structured CdS films

Nano-structured CdS was fabricated in crystalline, porous and fiber forms. The fabrication and characterization of these films are described below.

3.1. Nano-crystalline CdS

CdS films were fabricated by three different techniques namely, solution growth (type A), sonochemical (type B) and microwave-assisted synthesis (type C).

For types B and C, nano-crystalline CdS was first prepared in powder form by sonochemical and microwave methods. SEM micrographs of the CdS powder obtained by sonochemical and microwave synthesis methods showed spherical particles, 15 nm in size. The X-ray diffraction pattern of the nano-crystalline CdS powder shows peaks at 2θ positions of $27^\circ, 44^\circ$ and 52° corresponding to the (1 1 1), (2 2 0) and (3 1 1) planes of the cubic CdS phase, respectively. The XRD patterns obtained match with the JCPDS data (10-0454 Hawleyite). Sonochemical method involves ultrasound irradiation of the sample during synthesis while microwave method involves microwave irradiation. Sonochemistry is driven by acoustic cavitation, formation, growth, and implosive collapse of bubbles in liquids irradiated with high-intensity ultrasound. Sonochemical synthesis takes place when a strong acoustic field is applied to an aqueous solution leading to cavity filled microbubbles. Energy is transferred upon the growth and collapse of these microbubbles from the macroscale acoustic wave to the microscale vapor inside the bubbles. Extremely high pressures (hundreds of atmospheres) and temperatures (thousands of degree Kelvin) result from the high localization [14–16].

Next, types B and C CdS films were deposited on ITO-coated glass by dip coating in a suspension of the CdS powder. Type A films were deposited on ITO-coated glass by the solution growth method. Further details on the synthesis of these films can be found in our previous publication [5]. Particle size and the morphology of the films were studied with SEM. Figs. 5(a)–(c) show the electron micrographs of CdS films deposited by three different techniques. The solution growth films (Fig. 5(a)) have a smooth morphology with a particle size of 110 nm and the film thickness is equal to the particle size indicating a monolayer. Particle sizes in types B and C films, with a typical value of 15 nm, are an order of magnitude smaller than in type A. A hyperbolic band model [17] was used to estimate the energy gap as a function of particle size.

$$E = [E_g^2 + 2(\hbar)^2 E_g(\pi/r)^2/m^*]^{1/2}, \tag{1}$$

where E_g is the bulk band gap, r is the particle radius, and m^* is the electron effective mass. The particle size corresponds to an energy gap of 2.98 eV for sonochemically prepared CdS and shows a blue shift from the band gap of bulk CdS (2.4 eV).

X-ray diffraction measurements on the films indicated a cubic CdS phase. Optical absorption plots of CdS films on ITO-coated glass were recorded using a UV–VIS spectrophotometer. A comparison of optical absorption of CdS prepared by sonochemical, microwave and solution growth methods is shown in Fig. 6. The onset of absorption is at nearly 500 nm and a peak can be seen at close to 350 nm for type B, while a peak at nearly 375 nm was observed for microwave (type C). Brus describes this peak as 1S–1S transitions in CdS nanocrystals [18]. Thicker CdS films show a second peak that can be attributed to a second excitation level [19]. Compared to bulk CdS deposited by solution growth, the optical absorption spectra

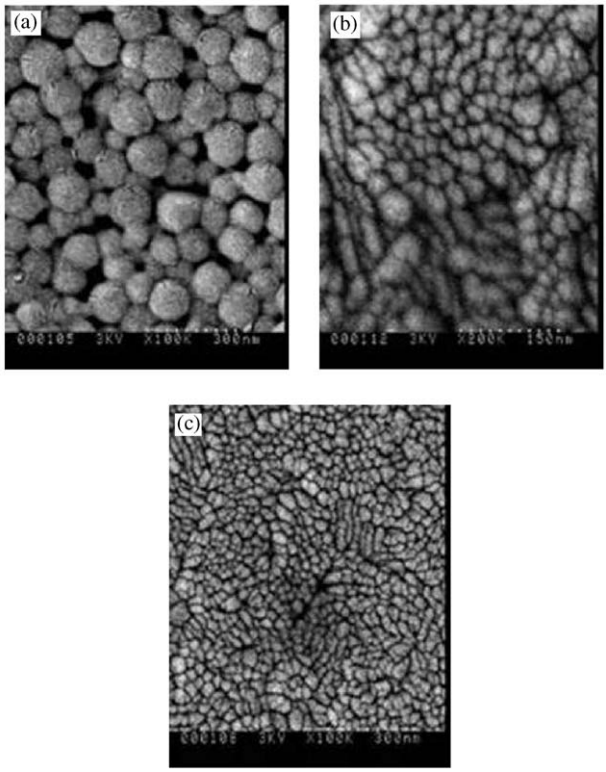

Fig. 5. (a) FE-SEM image of CdS film prepared by solution growth method on ITO-coated glass substrate. (b) FE-SEM image of CdS film prepared by sonochemical method on ITO-coated glass substrate. (c) FE-SEM image of CdS film prepared by microwave method on ITO-coated glass substrate.

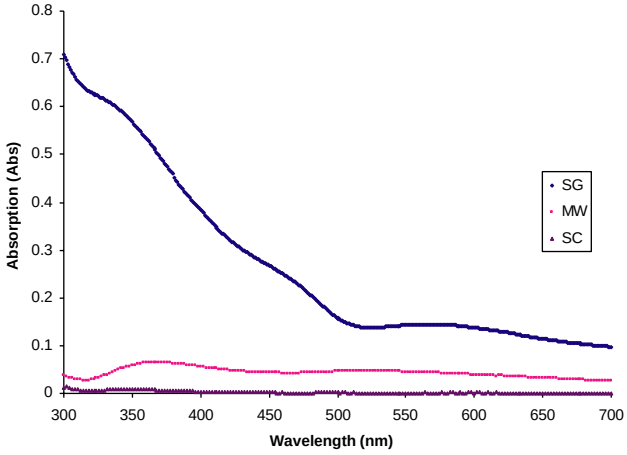

Fig. 6. Comparison of UV–vis absorption spectra of CdS films fabricated by sonochemical, microwave and solution growth methods on ITO-coated glass substrates.

show a blue shift as a result of quantum confinement effects. Solution growth CdS (type A) shows an optical absorption plot without a peak because of its larger crystallite size.

3.2. CdS–Ag Schottky diodes

Schottky diodes were formed by depositing polycrystalline (bulk) CdS and nano CdS on to ITO/glass substrates and subsequently depositing an Ag top contact. The representative I–V curve of bulk CdS Schottky diode is shown (Fig. 7). The characteristics of Schottky diodes on nano-CdS were substantially different from those on bulk CdS (Fig. 8). In theory, nano-CdS/Ag Schottky diodes should have a higher turn on voltage because of the larger band gap of nano-CdS, leading to a higher barrier height. Yet the Schottky diodes fabricated on bulk CdS showed a higher turn on voltage. We attribute this unexpected behavior to the fact that the nanoCdS films are just 20 nm thick and the depletion layer may therefore extend into ITO in this case. Since ITO is a degenerate semiconductor the effective depletion layer width would be the thickness of nano-CdS film. Thus, in parts of the Schottky barrier junction, the electrons would be able to "punch through", leading to a reduction in the effective turn-on voltage. In comparison, the CdS thickness in polycrystalline CdS layer is 110 nm.

Also, the I–V characteristics of the nano-CdS–Ag devices show some steps in the plot. This can be understood as follows. As the nano-CdS is expected to be completely depleted in this device the structure ITO/nano-CdS/Ag can be assumed to behave like a metal/insulator/metal. The step behavior could be due to coulomb blockade which is usually seen in such structures.

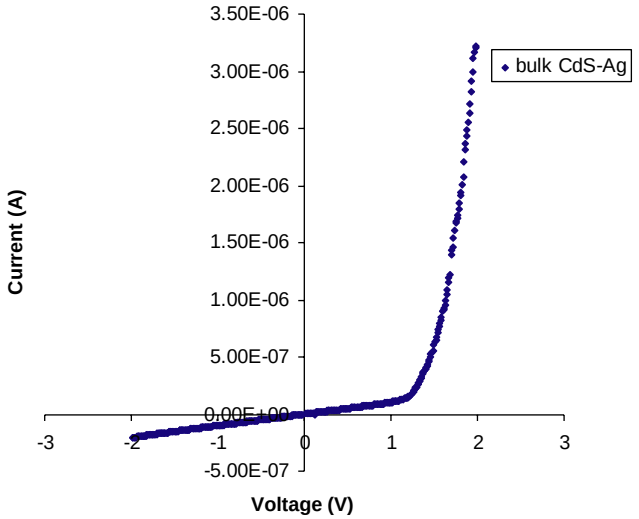

Fig. 7. Device configuration of a glass/ITO/n-nano-CdS/p-bulk CdTe/nano-CdTe/Au solar cell.

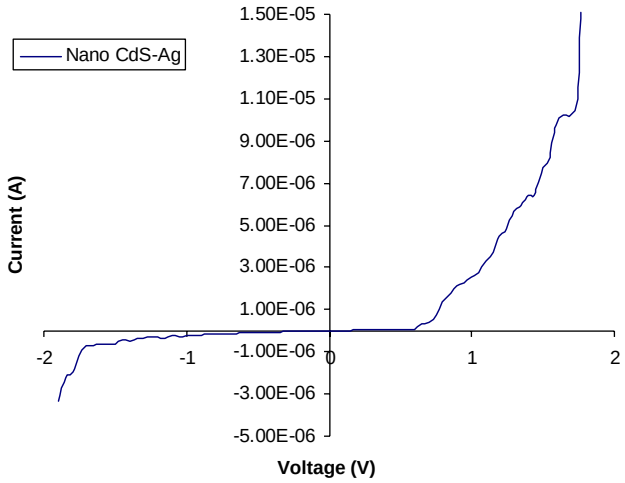

Fig. 8. *I–V* curve of a glass/ITO-bulk CdS–Ag Schottky diode.

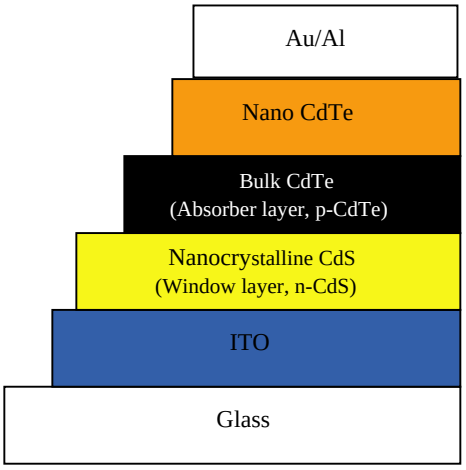

Fig. 9. *I–V* curve of a glass/ITO-nano CdS–Ag Schottky diode.

An application of nano-structured CdS to solar cells is illustrated in Fig. 9. Wider band gap makes it a more effective window layer. We are now in the process of using these larger band gap CdS films as window layers in the fabrication of experimental CdS–CdTe thin film solar cells.

3.3. Porous CdS films

Our objective is to make porous structure of CdS, deposit an absorber material like, copper indium diselenide, copper sulfide or cadmium telluride into the pores

and study the nano-structured, CdS-based heterojunction solar cells. This structure will allow for a device design involving an n-type material as a porous film and an extremely thin p-type absorber material filling the pores. The advantages are that the transport path for excited charge carriers in the absorber is reduced and at the same time, the optical path for photon absorption is increased. Due to the nano-porous structure of the cell, the distance that photoexcited electrons must travel within their lifetime can be reduced to less than 100 nm [20–22]. This design is also of critical importance in case of organic solar cells and hybrid junctions between inorganic and organic layers, where the traditional non-nano-structured designs are not beneficial for electron/hole transport. This is due to the fact that organic films tend to have short diffusion lengths and because of anisotropy, the conducting axis in the organic layer is not always along the film thickness.

Nano-porous CdS films were fabricated on a plastic substrate by using ultrasound irradiation during dip-coating. We term this process as ultrasound-assisted synthesis (UAS). Ultrasound irradiation was used as a tool to fabricate porous semiconductor films; it is known to cause significant effect on processes that occur at the surface of the solids immersed in liquids. Ultrasonic irradiation generates acoustic cavitation in the liquid, resulting in the formation of microbubbles. These microbubbles collapse on colliding with the solid surface causing erosion [23]. We believe that this process is responsible for the formation of a porous structure in our CdS films. In our method, the plastic substrate is dipped in CdS solution and exposed to ultrasound irradiation; it is thought that the microbubbles collapse at the surface of substrate and cause erosion of the CdS particles stuck to the substrate. Furthermore, since ultrasonicator generates acoustic cavitation uniformly throughout the liquid, the pores formed are uniform throughout the film.

SEM results showed uniform pore structure with a pore size of about 80 nm (Fig. 10). In contrast, the films deposited on ITO/glass substrates with UAS showed a crystalline film with voids. The optical absorption results of all these films showed a blue shift and an increase in the effective band gap (Figs. 11 and 12).

The method reported above is applicable to other materials and constitutes a practical route to prepare inexpensively, large area, flexible, lightweight, porous metal sulfide semiconductor films with an ordered nano-porous array structure. These films can serve as the underlying layers not only for the advantageous inorganic and organic solar cells designs as explained above, but also for sensors and other optoelectronic devices. This is because the large surface area in the nano-porous films can provide a highly active reaction interface and enhanced mass transfer properties.

3.4. *CdS fibers*

We fabricated nano-fibers of CdS by a combination of solution chemistry and ultrasound. High-intensity, high-frequency ultrasound irradiation was found to play a critical role in the crystallization and the preferential one-dimensional growth of the nano-wires of CdS in the solution. During ultrasound irradiation of liquid-powder slurries, cavitations and shock waves it creates can accelerate solid particles

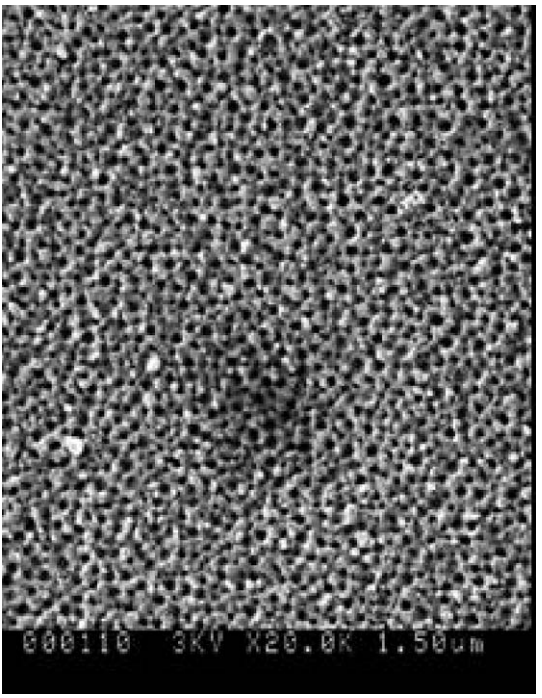

Fig. 10. FE-SEM image of porous CdS film on plastic substrate.

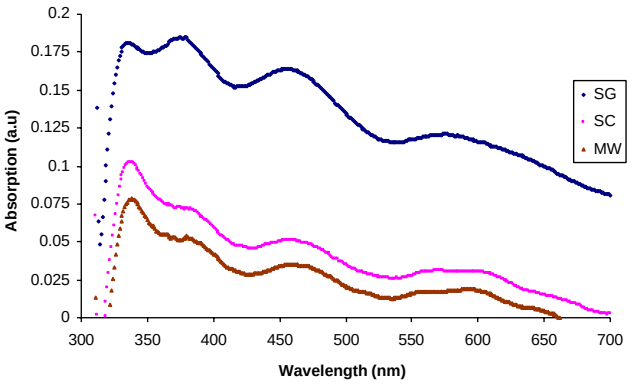

Fig. 11. Comparison of UV–vis absorption spectra of porous CdS films fabricated by sonochemical, microwave and solution growth methods on plastic substrates.

to high velocities. The inter-particle collisions that result are capable of inducing striking changes in morphology, composition, and reactivity of the solids. During the inter-particle collisions, the particles can be driven together at sufficiently high speeds to induce effective melting at the point of collision. It is thought that the energy generated during collision induced the crystallization and 1-D growth of CdS

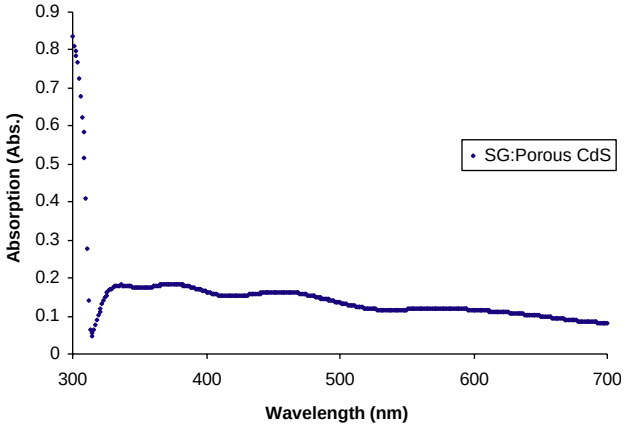

Fig. 12. Optical absorption of porous CdS films by solution growth method.

nanowires. It was observed that temperature, pressure, and reaction time played important roles in the solvothermal fabrication of nano-scale-sized CdS fibers. Only when the reaction was carried out in sealed systems, in the presence of high intensity and high frequency ultrasound, the CdS nano-fibers were formed. The physical effects of ultrasound cavitations in liquid–solid systems are primarily responsible for the enhancement of the generation of surface damage at the liquid–solid interface by shock waves or microjets and fragmentation of friable solids to increase the surface area. The impingement of microjets or shock waves on the solid surface creates the localized erosion, which is responsible for the ultrasound cleaning and many other sonochemical effects on heterogeneous reactions [24]. This phenomenon was also observed in the case of porous CdS films fabricated using an ultrasound-assisted synthesis, as described in the previous section.

The typical length of the fibers was about 1.5 μm and the diameter was about 80 nm. The fiber length was found to be a function of reaction time. The typical scanning electron micrograph of CdS nano-fiber is shown in Fig. 13. The optical absorption measurements of CdS fibers dispersed on an ITO/glass substrate indicate a broad hump around 475 nm and a peak at 330 nm (Fig. 14). These fibers are potential candidates for channels in thin film transistors and have applications in flexible, wearable and disposable electronics.

4. Nano-structured TiO_2 films

TiO_2 films were deposited on plastic substrates by the sol–gel method. The TiO_2 sol was prepared using the standard procedure starting with high-purity reagents, titanium tetra isopropoxide, isopropanol and nitric acid (70% redistilled). This method is based on the hydrolysis of metal alkoxides or ethoxides in alcoholic solutions in the presence of acid catalysts. The procedure for the preparation involved the dissolution of TTIP as precursor in isopropanol as a solvent, followed

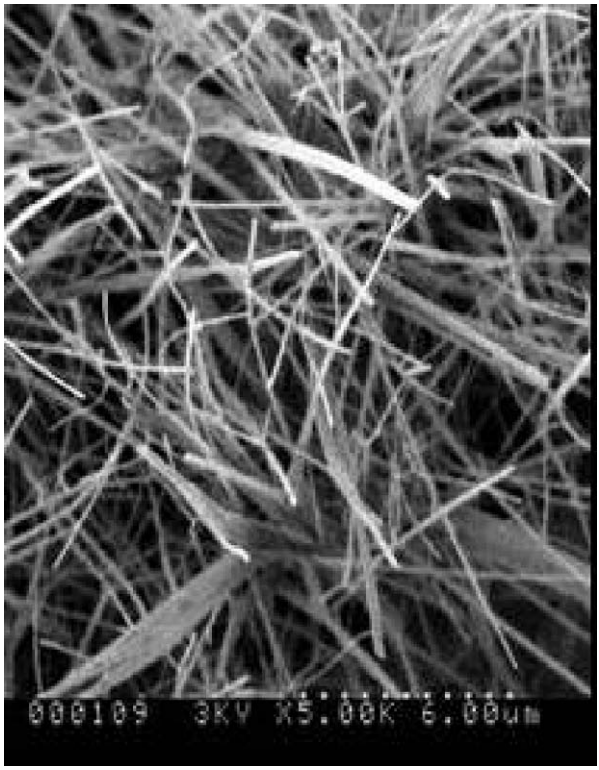

Fig. 13. FE-SEM image of CdS fibers on ITO-coated glass substrate.

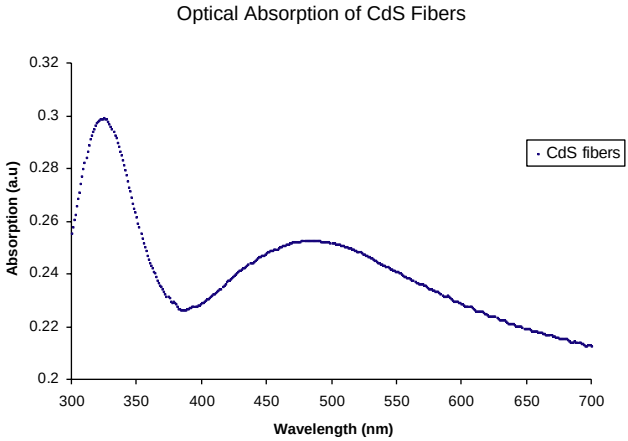

Fig. 14. Optical absorption of CdS fibers on ITO-coated glass substrate.

by adding deionized water and nitric acid (70%). The reaction was carried out with nitrogen gas flowing into the hood. TTIP was added to isopropanol and to this solution, deionized water was added dropwise while stirring. Nitric acid was added dropwise slowly to TTIP, isopropanol and deionized water while still stirring under the hood. The stirring was continued for 2 h and then the solution was covered with a parafilm and placed under the hood. In a typical preparation of 0.1 M TiO_2 sol, 1 ml of TTIP, 0.05 ml of HNO_3 (70% distilled), 0.1 ml of deionized water and 32.7 ml of isopropanol were used. The films were deposited by means of spin or dip coating (withdrawal rate 0.5 mm/s) on a clean substrate. Before coating, the substrates were cleaned with a flow of acetone and deionized water with intermediate drying in flowing nitrogen. After cleaning, substrates were either spin or dip coated. For obtaining the nano-porous films, subsequent to the coating process, the substrates were dried under hot water vapor; nitrogen was passed through a hot bubbler, with the humidity controlled by the flow rate of the nitrogen gas ($\approx$1.3 cm/s through the chamber). The humidity and temperature of the chamber were monitored with a digital hygrometer. The nano-crystalline TiO_2 films, on the other hand, were spin or dip coated from a TiO_2 sol (0.01 M) on to the plastic substrates and dried in ambient.

The material characterization of the films was performed using a Hitachi S-900 FE-SEM for studying morphology and pore structure. A Shimadzu UV-2501 UV–Vis spectrometer was used for optical absorption studies. The thickness of the films was measured using an Alpha step profilometer. The scanning electron micrographs (Figs. 15(a) and (b)) show a porous structure over large areas. The pore size was estimated to be 70 nm. The walls of the pores were found to be thicker than in case of films made via Benard-marangoni convection [25]. The scanning electron micrograph of a typical nano-crystalline TiO_2 film fabricated by drying the films in ambient is shown in Fig. 16. These films are smooth and have a particle size of about 10 nm. The optical absorption of the films was measured in the near UV and visible

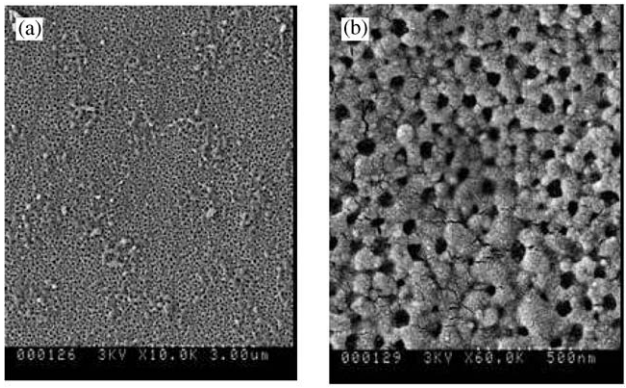

Fig. 15. (a) FE-SEM image of porous TiO_2 on plastic substrate, at low magnification. (b) FE-SEM image of porous TiO_2 on plastic substrate, at high magnification.

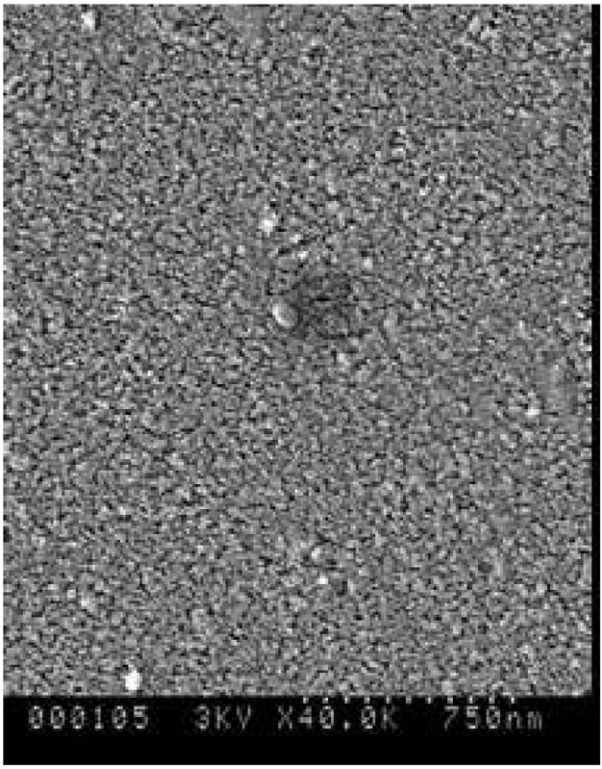

Fig. 16. FE-SEM image of Crystalline TiO_2 on plastic substrate.

range using a Shimadzu spectrometer. The spectral dependence, in general, shows one region of fundamental absorption edge (E_g) and the other region characterized by interference peaks at higher wavelengths. All of the three nano-porous films of different thicknesses showed a peak at 334 nm in the optical absorption spectra, but, as expected, the magnitude of absorption is higher in thicker films (Fig. 17).

Just as in case of porous CdS films, porous TiO_2 films can serve as the underlying layers for efficient solar cell designs. Absorber materials like copper indium diselenide, copper sulfide or cadmium telluride can be deposited into the pores of TiO_2 and nano-structured, heterojunction solar cells obtained. Also, the large surface area in the nano-porous films can provide a highly active reaction interface and enhanced mass transfer properties.

5. Conclusions

Nano-crystalline CdTe films were deposited on ITO coated glass substrates and characterized. The results indicated particle sizes of 10 nm and a blue shift in the

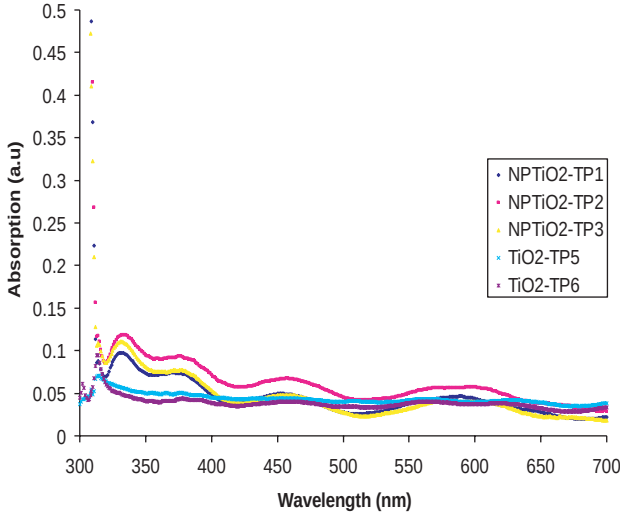

Fig. 17. Comparative UV–vis absorption spectra of porous and crystalline TiO_2 films on plastic substrates.

absorption with an effective band gap of 2.8 eV. This opens the possibility of using nano-crystalline n-type CdTe as a window layer in an n-CdTe/p-CdTe homojunction solar cell. Nano-crystalline CdS films on ITO-coated glass substrates exhibited particle sizes of 15 nm and an effective band gap of 2.98 eV as compared to the 2.4 eV value for the band gap of bulk CdS. This makes nano-crystalline CdS a better window material in an n-CdS/p-CdTe heterojunction solar cell. We are now in the process of evaluating these advantages by fabricating test structures of n-CdS/p-CdTe and n-CdTe/p-CdTe solar cells.

Porous CdS and porous TiO_2 films were deposited on plastic substrates by a self-assembly method. Typical pore sizes were 80 and 70 nm, respectively. These can be used in nano-structured solar cell configuration where the pores are filled with a p-type absorber material. Due to the nano-structured character of the absorber, the transport path for the light generated electrons in the absorber is reduced. At the same time, the optical path for photon absorption is increased due to multiple reflections.

Also, CdS fibers and nano-crystalline films of TiO_2 on plastic substrates were fabricated. Typical particle size in nano-crystalline TiO_2 was 10 nm and CdS fibers were about 80 nm wide and 1.5 μm long.

Acknowledgements

The authors thank the Kentucky Science and Engineering foundation for support through Grants KSEF-148-502-02-27 and KSEF-148-502-03-68. One of the authors

(VKR) thanks Dr. Shaik Jeelani, Director, T-CAM, Tuskegee University for support and encouragement.

References

[1] G.M. Whitesides, Bartosz Grzybowski, Science 295 (2002) 2418–2421.
[2] Xiangfeng Duan, Chunming Niu, Vijendra Sahi, Jian Chen, J.W. Parce, S. Empedocles, J. Goldman, Nature 425 (2003) 274–278.
[3] M.C. McAlpine, R.S. Friedman, Song Jin, Keng-hui Lin, Wayne U. Wang, C.M. Lieber, Nano Lett. 3 (2003) 1531–1535.
[4] K. Ernst, A. Belaidi, R. Konenkamp, Semicond. Sci. Technol. 18 (2003) 475.
[5] V.P. Singh, R.S. Singh, G.W. Thompson, V. Jayaraman, S. Sanagapalli, V.K. Rangari, Sol. Energy Mater. Sol. Cells 81 (2004) 293–303.
[6] V.P. Singh, J.C. McClure, Sol. Energy Mater. Sol. Cells 76 (2003) 369–385.
[7] V.P. Singh, O.M. Erickson, J.N. Chao, J. Appl. Phys. 78 (7) (1995) 4538–4542.
[8] D.L. Linam, V.P. Singh, J.C. McClure, G.B. Lush, X. Mathew, P.J. Sebastian, Sol. Energy Mater. Sol. Cells 70 (2001) 335–344.
[9] M.E. Calixto, J.C. McClure, V.P. Singh, P.J. Sebastian, Sol. Energy Mater. Sol. Cells 63 (4) (2000) 325–334.
[10] X. Mathew, J.P. Enriquez, P.J. Sebastian, J.C. McClure, V.P. Singh, Sol. Energy Mater. Sol. Cells 63 (4) (2000) 355–365.
[11] Wei Chen, D. Grouquist, J. Roark, J. Nanosci. Nanotechnol. 2 (2002) 47.
[12] V.P. Singh, A. Aguilera, A. Garcia, D.C. Morton, IEEE Trans. Electron Dev. 48 (10) (2001) 2242–2248.
[13] Mingyuan Gao, C. Lesser, S. Kirstein, H. Mohwald, A.L. Rogach, H. Weller, J. Appl. Phys. 87 (2000) 2297.
[14] Cuiling Gong, D.P. Hart, J. Acoust. Soc. Am. 104 (1998) 2675–2682.
[15] K.S. Suslick, Sonochemistry: a physical perspective, AIP Conference Proceedings, Nonlinear Acoustics at the Turn of the Millennium, Vol. 524, 2000, pp. 95–104.
[16] K.S. Suslick, Sonochemistry, Science 247 (1990) 1439–1445.
[17] J.A. Akintunde, Phys. Status Solidi. A 179 (2000) 363.
[18] L. Brus, J. Chem. Phys. 90 (1986) 2555.
[19] Y. Wada, H. Kuramoto, J. Anand, T. Kitamura, T. Sakata, H. Mori, S. Yanagida, J. Mater. Chem. 11 (2001) 1936.
[20] Yu, T. Isobe, M. Senna, Mater. Res. Bull. 30 (1995) 975.
[21] D.J. Lockwood, A. Wang, B. Bryskiewicz, Solid State Commun. 89 (1994) 587.
[22] K. Ernst, A. Belaidi, R. Konenkamp, Semicond. Sci. Technol. 18 (2003) 475.
[23] A. Vogel, W. Lauterborn, R. Timm, J. Fluid Mech. 206 (1989) 299.
[24] K.S. Suslick (Ed.), Ultrasound: Its Chemical, Physical and Biological Effects, VCH, Weinheim, 1988.
[25] R.S. Singh, C.A. Grimes, E.C. Dickey, Mater. Res. Innov. 5 (2002) 178.